PROCEEDINGS, Thirty-Fourth Workshop on Geothermal Reservoir Engineering
Stanford University, Stanford, California, February 9-11, 2009
SGP-TR-187

FRACTURES, STRESS AND FLUID FLOW PRIOR TO STIMULATION OF WELL 27-15, DESERT PEAK, NEVADA, EGS PROJECT

Nicholas C. Davatzes[1] and Stephen H. Hickman[2]

[1]Temple University
EES, 1901 N. 13th St
Philadelphia, PA, 19122, USA
e-mail: Davatzes@temple.edu

[2]U.S. Geological Survey
345 Middlefield Road, MS977
Menlo Park, CA 94025, USA
e-mail: hickman@usgs.gov

ABSTRACT

A suite of geophysical logs has been acquired for structural, fluid flow and stress analysis of well 27-15 in the Desert Peak Geothermal Field, Nevada, in preparation for stimulation and development of an Enhanced Geothermal System (EGS). Advanced Logic Technologies Borehole Televiewer (BHTV) and Schlumberger Formation MicroScanner (FMS) image logs reveal extensive drilling-induced tensile fractures, showing that the current minimum compressive horizontal stress, S_{hmin}, in the vicinity of well 27-15 is oriented along an azimuth of 114±17°. This orientation is consistent with the dip direction of recently active normal faults mapped at the surface and with extensive sets of fractures and some formation boundaries seen in the BHTV and FMS logs. Temperature and spinner flowmeter surveys reveal several minor flowing fractures that are well oriented for normal slip, although over-all permeability in the well is quite low. These results indicate that well 27-15 is a viable candidate for EGS stimulation and complements research by other investigators including cuttings analysis, a reflection seismic survey, pressure transient and tracer testing, and micro-seismic monitoring.

1 INTRODUCTION

Several studies in a wide range of tectonic settings have demonstrated that fractures that are optimally oriented and critically stressed for frictional failure often dominate fluid flow in low-porosity crystalline rocks (Barton, 1995; Ito and Zoback, 2000). Similar observations and analyses from a high temperature fault-hosted geothermal system at Dixie Valley, Nevada (Barton et al., 1998; Hickman et al., 1998, 2000) indicate that actively slipping (i.e., shearing) fractures help maintain geothermal reservoir permeability despite crack sealing and other geochemical fluid-rock interactions that should destroy that permeability. Thus, in geothermal fields under high differential stress (such as Dixie Valley), low-pressure hydraulic stimulation (*i.e.*, below the least principal stress) will trigger slip and dilatation along self-propping shear fractures that enhance formation permeability in otherwise hot but impermeable rocks. Thus, characterization of the geometrical and hydrologic properties of natural fractures in relation to the *in-situ* state of stress is critical to stimulation planning and evaluation for EGS projects underway at Desert Peak, Nevada, and elsewhere (see MIT, 2006).

As demonstrated by the Coso, California, EGS project, preparing for stimulation and development of an EGS well requires a complete characterization of borehole geology, hydrology, and stress state (Davatzes *et al*., 2006). Elements of this evaluation include direct measurements of 3-D stress orientations and magnitudes, the distribution, orientation and hydrologic properties of natural fractures, the locations of primary structures such as bedding, foliation and formation contacts, and rock properties from geophysical logs and testing of core. These data are used to determine formation characteristics including the distribution of fracture permeability versus depth, variations in lithologic and mechanical rock properties, and the propensity for frictional failure along the pre-existing natural fracture population during hydraulic stimulation.

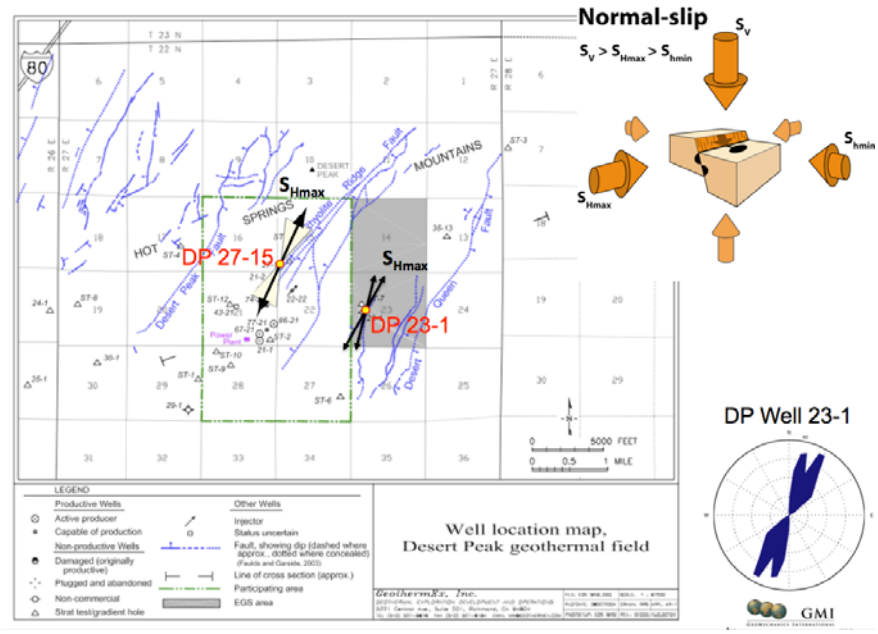

Figure 1: Mapped fault traces in the vicinity of the Desert Peak Geothermal Field with the orientation of the maximum horizontal principal stress, S_{Hmax}, inferred from observations of borehole failure in wells 27-15 and 23-1. Analysis of stress directions in well 23-1 is from Robertson-Tait et al. (2004). Fault traces mapped by Faulds and Garside (2003).

Consequently, a complete suite of geophysical logs has been acquired for structural and stress analysis of well 27-15 in preparation for stimulation and development of an EGS adjacent to the Desert Peak Geothermal Field, Nevada (Figure 1). Once completed, well 27-15 will provide pressure support to the Desert Peak Geothermal Field. Logs acquired to date include image logs to characterize natural fractures and stress-induced borehole failure, density and velocity logs to constrain rock strength and the vertical stress, and temperature/pressure/spinner (TPS) logs to reveal fluid entry/exit points. Image logs used in well 27-15 were obtained from the Advanced Logic Technologies ABI85 BHTV and the Schlumberger FMS.

2. BHTV AND FMS ANALYSIS

2.1 Methods of Image Log Analysis

Following methods described by Davatzes and Hickman (2009), FMS and BHTV logs from Desert Peak well 27-15 were used in combination to determine the orientation and distribution of bedding and foliation, lithologic transitions, and natural fractures. In addition, the stress state in the geothermal field was investigated by mapping the orientation and distribution of drilling-induced borehole failure manifested as tensile fractures in the borehole wall (see Moos and Zoback, 1990; Zoback et al., 2003; Davatzes and Hickman, 2005, 2009).

Whereas the best image resolution over large intervals of the borehole was achieved with the FMS, the FMS logs from well 27-15 provided very limited pad coverage due to the large borehole diameter, which ranged from ~12.25 to >21.9 inches with a mean of ~14.5 in. Thus, as shown in Figure 2, the FMS pads revealed on average only 9-10% of the borehole circumference. In contrast, BHTV images from well 27-15 provided 360º azimuthal coverage, although poor borehole conditions led to some depth intervals of poor image quality (Figure 2b and c).

2.2 Image Log Analysis of Bedding, Foliation, and Natural Fractures

Combining the different attributes measured by the FMS and BHTV (Davatzes and Hickman, 2009) enabled bedding contacts to be identified and aided in distinguishing bedding and foliation from natural fractures. In particular, bedding and foliation were identified on the basis of closely spaced, sub-parallel traces of uniform reflectivity and resistivity contrast with the borehole wall.

These observations were integrated with analyses of drill cuttings by Lutz *et al.* (2009), the rate of penetration during drilling, and other geophysical logs, including P-wave sonic velocity, rock density, and natural gamma ray (Figure 3) to reveal the precise locations of formation transitions, variations in rock physical properties, and changes in bedding attitude.

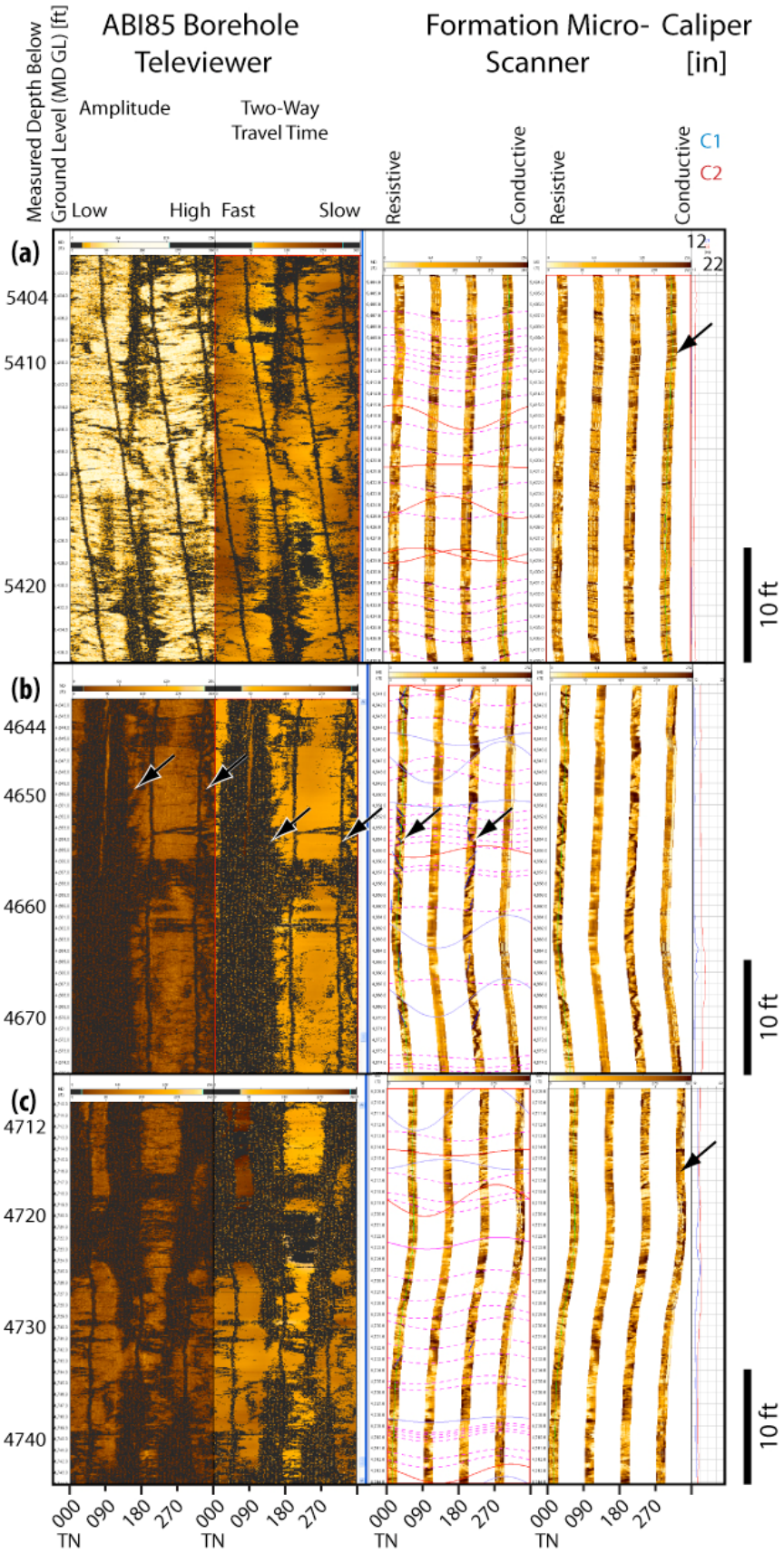

Figure 2: Examples of natural fractures, bedding, and tensile fractures in the BHTV (left) and FMS (right) dynamically normalized images from well 27-15. Logs were interpreted in conjunction, but example picks are shown only in the FMS image where dashed lines represent interpreted bedding surfaces, solid lines indicate interpreted natural fractures, and short near-vertical lines indicate borehole-induced tensile fractures. (a) Natural fractures and bedding: There is a clear variation in BHTV image log quality that corresponds to a change in rock type (indicated by the arrow). Similar changes in image log character that persist over larger zones correspond closely with mineralogical changes identified in the mud log and cuttings analysis by Lutz et al. (2009). Note that bedding picks were limited to the minimum necessary to define structural dip domains. (b) Drilling-induced tensile fractures, which occur on diametrically opposed sides of the borehole due to symmetrical borehole stress concentration (arrows). (c) Image logs in proximity to the dominant fluid flow zone revealed by temperature logs and an injection spinner (arrow; see discussion in text). A pair of poorly imaged fractures occur in a washed out section of borehole between 4718 and 4722 ft Measured Depth below ground level (MD) showing true dips between 40° and 64°, and true dip direction azimuths between 104 and 094 respectively. A change in bedding attitude occurs across this zone suggesting it has significant offset. Perturbations in the Density, Velocity, and ROP logs are also evident at this depth (Figure 3).

In Figure 3, we ranked both the quality of the image logs and the quality of our natural fracture picks to assess how well we capture the characteristics of different depth intervals. The former is ranked from 1 (best) to 4 (unusable or absent). The latter is ranked on a scale from A to C. A indicates the highest quality, least ambiguous pick derived from a structure represented as a continuous trace along the borehole wall and with a relatively large apparent aperture. Structures assigned a quality ranking of C required a more subjective interpretation, usually involving connecting discontinuous or ambiguous line segments to define the structure trace. Conservative picking in this study probably underestimates the total number of fractures, but leads to a more reliable analysis of structure orientation and distribution. Figure 3 reveals significant differences in both fracture density and attitude between stratigraphic units.

For high quality fracture picks, we also measured the apparent aperture, or thickness, of the fracture as seen in the image log. Apparent aperture was estimated as the thickness of a zone of relatively high electrical conductivity in the FMS image or a zone of low amplitude acoustic reflectivity in the BHTV image. Although apparent aperture can be proportional to true fracture aperture in both types of logs, the measured thickness does not simply equate to the hydraulic or mechanical fracture aperture (for details see Cheung, 1999; Davatzes and Hickman, 2009). Note that fracture density is strongly related to rock type and can vary significantly across formation boundaries (Figure 3).

2.3 Stress Orientation from Borehole Failure:

Concentration of tectonic stress around the borehole wall can induce failure of the rock adjacent to the borehole. Field studies have demonstrated that these induced structures reliably record the orientations of the horizontal principal stress axes (see Moos and Zoback, 1990; Zoback et al., 2003; Davatzes and Hickman, 2005). Numerous drilling-induced tensile fractures are recorded in the image logs from well 27-15. Tensile fractures occur along an azimuth where the concentration of tectonic stresses at the borehole wall plus thermal stress due to cooling of the borehole during drilling produce a tensile "hoop" (or circumferential) stress that exceeds the tensile strength of the rock.

Continuous borehole deviation surveys provided by both the FMS and BHTV tools were checked against "single-shot" borehole directional surveys and with each other (in the extensive regions of image overlap) to verify accurate image orientations. The borehole directional surveys from the FMS and BHTV tools were also used to correct the apparent strike and dip of natural fractures intersected by the borehole to their true strike and dip. Borehole deviation over the logged depth intervals range from 2º to 8º from vertical, which allowed us to neglect corrections from apparent to true stress directions required for highly deviated boreholes (see Peska and Zoback, 1995). In this regard, we also note that the orientation of the horizontal principal stresses do not vary with the deviation angle or deviation direction, as expected for near-vertical boreholes. Following the method of Davatzes and Hickman (2005), tensile fractures were only picked when they occurred as pairs on opposing sides of the borehole 180° apart (*e.g.*, Figure 2b). The orientation of S_{hmin} at any given depth was determined from the average azimuth of each pair.

The vertically integrated orientation of the least horizontal principal stress, S_{hmin}, was calculated by averaging the orientation of these drilling-induced tensile fractures weighted by their cumulative lengths. Using this methodology, analysis of drilling-induced tensile fracturing in the image logs from well 27-15 indicates that S_{hmin} is oriented 114±17°. Previous work in well 23-1, located 1.3 miles E-SE of well 27-15 has shown that S_{hmin} from drilling-induced tensile fractures and breakouts is approximately 119±15°, with a subset oriented 128±13° (Figure 1; Note that S_{Hmax} as shown in this figure is oriented 90º from S_{hmin}). Thus, there is excellent agreement in stress orientations obtained between wells 27-15 and 23-1.

In both wells, the stress orientations are consistent with normal slip on a set of ESE and WNW dipping normal faults, as mapped at the surface (Figure 1). This includes the trace of the Rhyolite Ridge Fault Zone that outcrops in fractured and altered basalt in the well 27-15 drilling sump. Similarly, most formations imaged in the BHTV and FMS logs from well 27-15 include significant sub-populations of fractures that are well oriented for normal faulting given the current direction of S_{hmin} (see Figure 3, "Natural Fractures" panel; and Figure 4a). In particular, note that there are significant sub-populations of natural fractures that are well oriented for normal slip in each of the three intervals being considered for EGS stimulation in well 27-15 (Figure 4d, e and f).

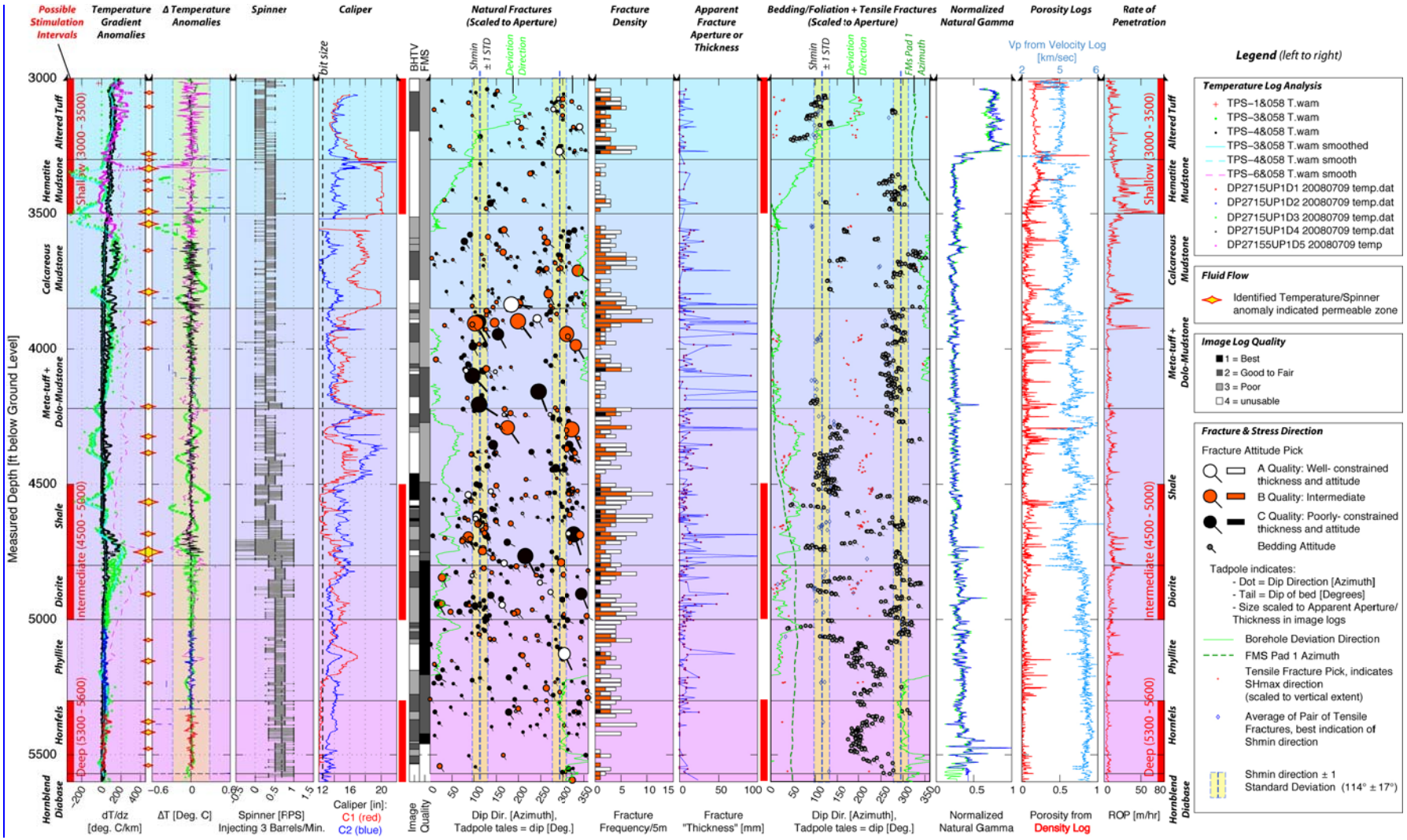
Possible Stimulation Intervals
Temperature Gradient Anomalies
Δ Temperature Anomalies
Spinner
Caliper
Natural Fractures (Scaled to Aperture)
Fracture Density
Apparent Fracture Aperture or Thickness
Bedding/Foliation + Tensile Fractures (Scaled to Aperture)
Normalized Natural Gamma
Porosity Logs
Rate of Penetration
Measured Depth [ft below Ground Level]
Shallow (3000 - 3500)
Intermediate (4500 - 5600)
Deep (5300 - 5600)
Altered Tuff
Hematite Mudstone
Calcareous Mudstone
Meta-tuff + Dolo-Mudstone
Shale
Diorite
Phyllite
Hornfels
Hornblend Diabase
dT/dz [deg. C/km]
ΔT [Deg. C]
Spinner [RPS] Injecting 3 Barrels/Min.
Caliper [in]: C1 (red) C2 (blue)
Image Quality
Dip Dir. [Azimuth], Tadpole tales = dip [Deg.]
Fracture Frequency/5m
Fracture "Thickness" [mm]
Normalized Natural Gamma
Porosity from Density Log
ROP [m/hr]
Legend (left to right)
Temperature Log Analysis
TPS–1&058 T.wam
TPS–3&058 T.wam
TPS–4&058 T.wam
TPS–3&058 T.wam smoothed
TPS–4&058 T.wam smooth
TPS–6&058 T.wam smooth
DP2715UP1D1 20080709 temp.dat
DP2715UP1D2 20080709 temp.dat
DP2715UP1D3 20080709 temp.dat
DP2715UP1D4 20080709 temp.dat
DP27155UP1D5 20080709 temp
Fluid Flow
Identified Temperature/Spinner anomaly indicated permeable zone
Image Log Quality
1 = Best
2 = Good to Fair
3 = Poor
4 = unusable
Fracture & Stress Direction
Fracture Attitude Pick
A Quality: Well- constrained thickness and attitude
B Quality: Intermediate
C Quality: Poorly- constrained thickness and attitude
Bedding Attitude
Tadpole indicates:
- Dot = Dip Direction [Azimuth]
- Tail = Dip of bed [Degrees]
- Size scaled to Apparent Aperture/ Thickness in image logs
Borehole Deviation Direction
FMS Pad 1 Azimuth
Tensile Fracture Pick, indicates SHmax direction (scaled to vertical extent)
Average of Pair of Tensile Fractures, best indication of Shmin direction
Shmin direction ± 1 Standard Deviation (114° ± 17°)

Figure 3: Compilation of well log data and analysis to date from well 27-15. Possible EGS stimulation intervals are indicated by heavy vertical red lines. Geologic formations are indicated as horizontal regions of constant color and are labeled along the left and right margins of the figure, based on the analysis by Lutz et al. (2009). In this and all other figures, the azimuths of features in the image log have been corrected for deviation of the borehole from vertical and corrected to true North. From left to right:

- *Temperature logs. Analysis of the logs includes filtering and smoothing to remove measurement artifacts or improve temperature resolution. Data that have been smoothed are distinguished in the legend. Data presented are:*
  - *(1) Temperature gradient*
  - *(2) Differential temperature*
  - *(3) Identified permeable zones (yellow diamonds)*
- *Spinner flowmeter log during fluid injection at 2.75 bbl/minute while logging down at 30 ft/min.*
- *Caliper log including the nominal bit size in the open hole interval (12-1/4 inches)*
- *Image log quality, which limits the completeness of vertical and azimuthal sampling of fractures, formation contacts, beds, and borehole wall failure*
- *Modified tadpole plot showing natural fracture dip direction versus depth. The head of the tadpole indicates the dip azimuth and the tail of the tadpole indicates the dip of the fracture plane. The colors of the tadpoles reflect the quality of the pick; in other words how well constrained the thickness and orientation of the fracture are. Also plotted are:*
  - *(1) Deviation direction (solid green line),*
  - *(2) Direction of S_{hmin} ± 1 standard deviation: ~114° ± 17° (vertical blue dashed lines and highlighted yellow regions),*
- *Natural fracture frequency per five meter bins (color coded by pick quality)*
- *Natural fracture apparent aperture, or thickness*
- *Modified tadpole plot showing bedding or foliation dip (head and tail defined as before). Also plotted are:*
  - *(1) Deviation direction (solid green line),*
  - *(2) FMS pad 1 azimuth (dashed dark green line),*
  - *(3) Direction of S_{hmin} ± 1 standard deviation (as before),*
  - *(4) Drilling-induced tensile fractures, scaled to their vertical extent (thin red lines).*
  - *(5) S_{hmin} direction from pairs of drilling-induced tensile fractures (blue diamonds).*
- *Natural gamma log, normalized to maximum value seen in individual logs (API). Colors represent different log runs.*
- *Sonic velocity (light blue) and density-derived porosity (red) from geophysical logs.*
- *Rate of penetration during drilling*

Based on the presence of normal faults mapped at the surface and the similarity between normal fault dip direction and S_{hmin} azimuth, we tentatively assume that there is a normal faulting stress regime in the vicinity of wells 27-15 and 23-1. However, this *a priori* assumption cannot be verified without direct measurement of the horizontal stress magnitudes; thus, the potential role of strike-slip faulting during fracture stimulation cannot yet be assessed. A mini-hydraulic fracturing test is planned in well 27-15 as part of the Desert Peak EGS Project and will be used to measure the magnitude of S_{hmin}. When combined with a full, 3-D stress and geomechanical analysis, this will allow us to compute the proximity of natural fractures seen in these image logs (and mapped at the surface) to frictional failure, as needed for planning and evaluation of an EGS hydraulic stimulation.

In combination with measurements of S_{hmin} magnitude from a mini-hydraulic fracturing test, it is often possible to use observations of the depth distribution and geometry of borehole breakouts to constrain the magnitude of S_{Hmax} (e.g., Moos and Zoback, 1990; Davatzes and Hickman, 2005). Well 27-15 is enlarged over much of the existing open-hole section, likely due in part to borehole breakout formation. Although there are possible indications of breakouts having formed at some depths in the image logs, the enlargement of the borehole from 12.25 inches to more than 20 inches has degraded image quality and limited our ability to identify breakouts with confidence and use their width to constrain S_{Hmax} magnitudes. Given the identification of breakouts in well 23-1 by Robertson-Tait *et al.*, (2004), the current enlarged and washed-out state of well 27-15, and increased depth, it is possible that breakouts will occur and be imaged if a sidetrack is drilled off well 27-15 and logged with the ABI85 BHTV.

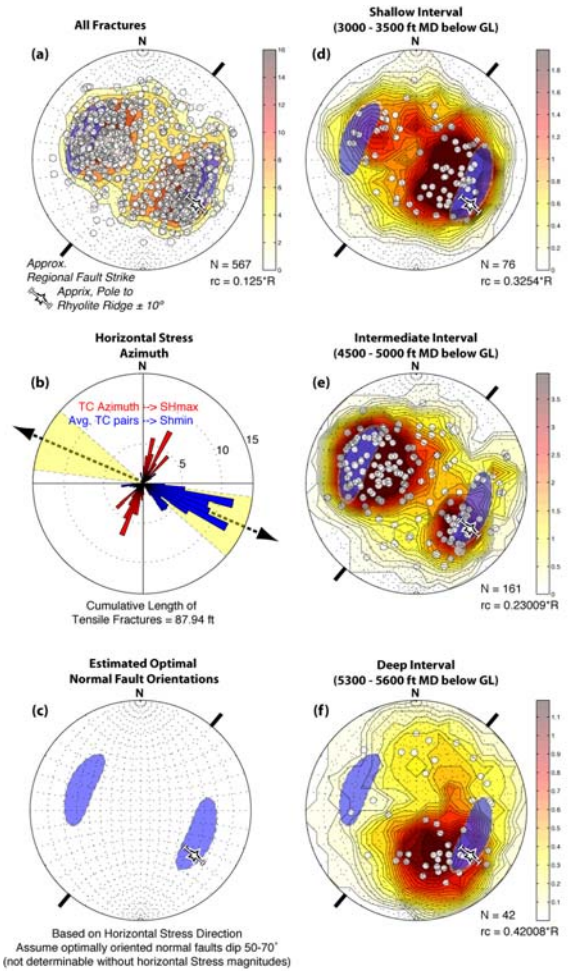

Figure 4: Lower hemisphere, equal area stereographic projections showing stress directions and poles to natural fractures seen in image logs from well 27-15 (a) for the entire well and (d), (e) and (f) over three potential EGS stimulation intervals. In (b), the black arrows show the azimuth of S_{hmin} from drilling-induced tensile fractures, with ± 1 standard deviation shown in yellow. As illustrated in (c), the blue shaded areas in each figure indicate poles to planes that are well oriented for normal faulting inferred from the current direction of S_{hmin}. Approximate regional fault strike and pole to the Rhyolite Ridge Fault inferred from mapping (Faulds and Garside (2003) and interpreted reflection seismic survey (Lutz et al., 2009) are shown as labeled in (a).

3. FLUID FLOW INFERRED FROM TEMPERATURE-PRESSURE-SPINNER LOGS

Static and injecting TPS logs in well 27-15 reveal minor pre-stimulation fluid exit/entry points within an extensive near-isothermal zone extending from approximately 3,000 ft Measured Depth below ground level (MD) to total depth at 5,627 ft MD (Figure 3). As described in more detail by Davatzes and Hickman (2009), such fluid flow anomalies are identified from local perturbations in temperature gradient or absolute temperature after the data are filtered and smoothed, as illustrated schematically in Figure 5 (see also Sorey, 1971; Drury *et al.*, 1984; Drury and Jessop, 1987; Cornet, 1989; Barton *et al.*, 1995; Barton *et al.*, 1998; Ito and Zoback, 2000; Evans *et al.*, 2005).

Comparison of static equilibrated and non-equilibrium temperature logs from well 27-15 helps identify flow zones that are connected to the larger-scale naturally permeable network, as these features have a pronounced, persistent impact upon the borehole thermal profile. Temperature anomalies associated with short-term fluid injection or recently disturbed (non-equilibrium) temperature logs indicate fractures that may host significant local permeability but are isolated from the larger hydrothermal system. Temperature anomalies are indicated in Figure 3 by yellow diamonds. These temperature logs are very sensitive to even minor fluid inflow and outflow and, thus, tend to identify a greater number of permeable zones than do the spinner logs. We primarily used temperature gradient and ΔT anomalies to identify zones of permeability in well 27-15.

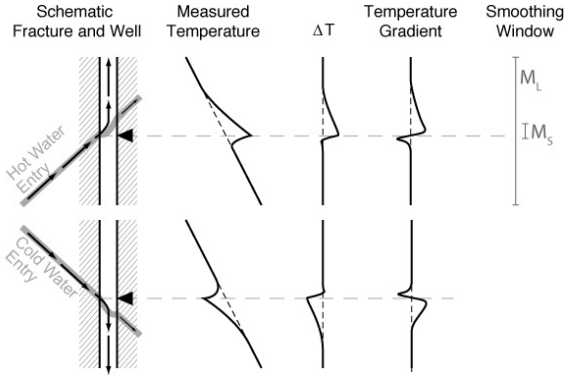

Figure 5: Conceptual model for thermal anomalies associated with upward flowing hot fluids (top) and downward flowing cold fluids (bottom) due to buoyancy-driven flow of hot or cold fluids along a fracture intersecting an open borehole (see Davatzes and Hickman, 2009, for details). (Note: Anomalies can also resolved in cased intervals, but the perturbation will be more symmetric in depth.)

A single prominent step in the spinner log during injection at ~2.75 bbl/minute reveals the most significant fluid exit point at ~4720 ft MD (Figure 3). (Note that the slow injection rate and large and

variable borehole diameter make further spinner interpretation difficult.) This zone is also associated with a persistent temperature gradient and ΔT anomaly as seen in equilibrated temperature logs. Several additional permeable zones are evident in the static temperature logs, including significant short-wavelength anomalies at: 3054 ft, 3360 ft, 3497 ft, 3535 ft, 3777 ft, 4225 ft, 4394 ft, 4580 ft, 4737 ft, and 5142 ft MD.

4. DISCUSSION: PERMEABLE ZONES AND STIMULATION OPTIONS

At shallow depths, a high temperature gradient persists from the water table to ~3500 ft MD, indicating relatively low permeability (see Robertson-Tait et al. 2004). The transition from high temperature gradients above this depth to near isothermal conditions below is associated with mineralogical transitions from smectite to illite-smectite to illite dominated clays (Figure 6; Lutz et al., 2009). This is consistent with cap rock alteration producing and maintaining low permeability, as discussed for the Coso Geothermal Field by Davatzes and Hickman (2005).

Static and injecting TPS logs reveal multiple fluid exit points within the extensive near-isothermal (~210°C) zone extending from approximately 3,500 to total depth at 5627 ft MD (Figure 3). Although most of these are relatively minor, they do indicate relatively permeable zones that correlate with either rock type transitions or pre-existing natural fractures. The most pronounced fluid exit point at ~4720 ft MD occurs just above the transition from shale to diorite and is associated with an increase in illite-chlorite content and quartz alteration at approximately 4737 ft MD (Figure 3 and 6; Lutz et al., 2009). This fluid loss zone is also associated with several significant, large-aperture fractures that are well orientated for slip as well as a zone of low P-wave velocity, a gradual rise in natural gamma, a localized zone with high rate of penetration and a change in dip of bedding and/or foliation (Figure 3).

The prominent fluid loss zone at ~4720 ft MD is roughly coincident with a minor rotation in tensile fracture azimuth of nearly ~50° (Figure 3), suggesting a perturbation of the horizontal principal stresses perhaps due to recent slip on nearby fractures (see Hickman *et al.*, 2000, and references therein). Several other fluid flow anomalies are also associated with stress rotations, including those at 4225 ft and 4000 ft MD.

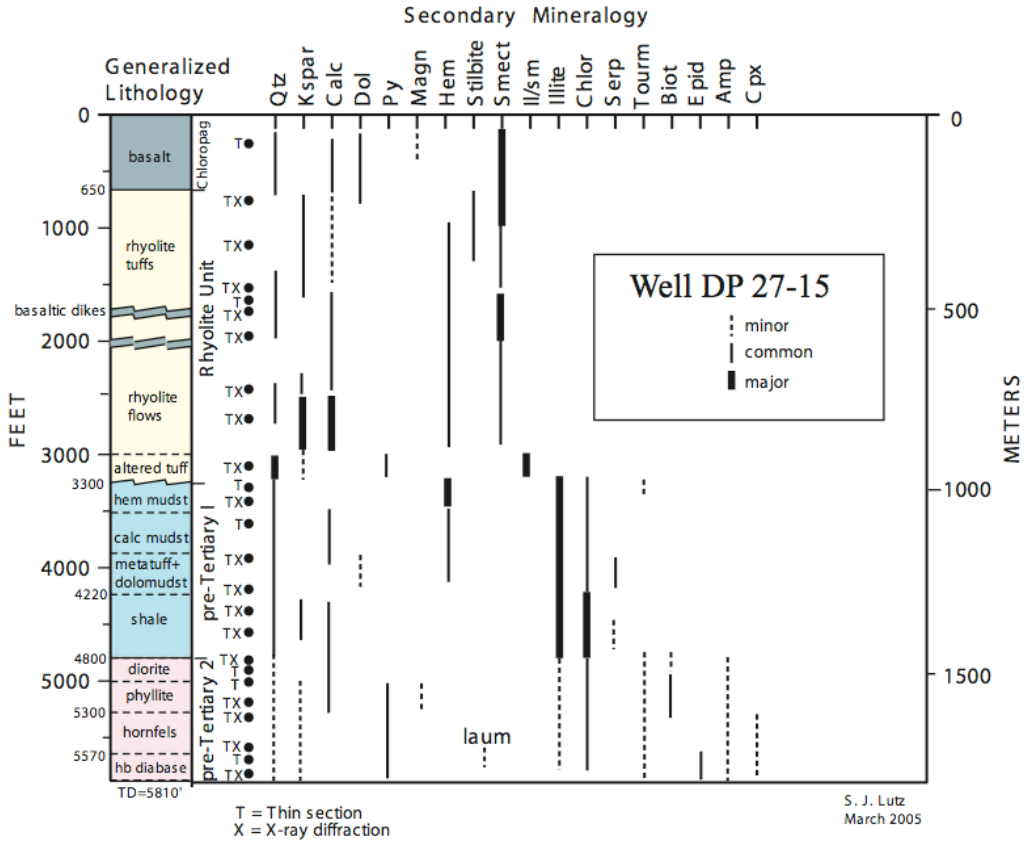

Figure 6: Rock type and alteration mineralogy of Well 27-15 based on drill cuttings analyses (Lutz et al., 2009)

As shown in Figure 3, several intervals are now being considered for hydraulic stimulation of well 27-15 on the basis of borehole condition, large-scale reservoir structure and hydrology, and a number of local geologic criteria applicable to the immediate borehole environment. These local geologic criteria include: (1) the interval should be below the zone of smectite alteration because smectite-filled fractures are not prone to dilation/permeability enhancement during slip (Davatzes and Hickman, 2005 and references therein); (2) the interval exhibits high formation temperatures and is below any shallow conductively heated, low temperature cap (see temperature profile in Robertson-Tait *et al.*, 2004); (3) the interval intersects highly stressed, slightly permeable natural fractures well oriented for frictional shear failure; and (4) the mechanical properties of rocks in the interval are such that they would be susceptible to "self-propping" dilatation and permeability enhancement during fluid injection and shearing (Brown, 1987; Teufel, 1987; Willis-Richards, 1996). Characteristics of three potential stimulation intervals are summarized immediately below.

1. *Shallow interval: 3000 to 3500 feet MD and just beneath the current casing shoe (Figures 3 and 4d)*

This interval hosts two or three large temperature anomalies indicating permeable zones that are not expressed or are only slightly expressed in the spinner response. The borehole diameter is highly enlarged and variable in this interval. The fracture system is most poorly characterized here due to the poor image log quality resulting from borehole enlargement. Nevertheless, there are a significant number of fractures in this interval that appear well oriented for normal faulting in the present stress field.

2. *Intermediate interval: 4500 to 5000 feet MD (Figures 3 and 4e)*

This interval hosts the highest permeability zone (at ~4720 ft MD) encountered by the borehole and several additional permeable zones. This highly permeable interval is characterized by high fracture density and fractures with significant apparent aperture that appear well oriented for normal slip. This interval also coincides with a major lithologic and structural transition and several distinctive changes in geophysical well log response, as noted above. Work by Lutz *et al*. (2009) suggests a thrust fault defines the transition at 4800 ft MD from shale to diorite.

3. *Deep interval: 5300 to 5600 feet MD (Figures 3 and 4f)*

This interval hosts several minor permeable zones and overall a lower fracture density. The interval is characterized by relatively low and uniform drilling ROP, high sonic velocity, and low density porosity that together indicate good formation integrity. The presence of a change in bedding/foliation dip and rock type (Figure 6) at 5290 feet MD (Figures 3) might indicate either an erosional angular unconformity or a fault juxtaposing units with different dips. Several depths within this interval are associated with minor temperature anomalies in some of the temperature logs (Figure 3). There are some fractures in this interval that are well oriented for normal faulting in the present stress field, albeit not as many as seen in the two shallower intervals. However, the presence of hornfels and hornblende diabase in this interval (as opposed to predominately softer phyllites, shales and mudstones above) with high P-wave velocities, low ROP and low density porosity indicates that these units are mechanically stronger than the overlying units and more likely to generate and maintain dilatation-induced permeability increases from shearing induced during hydraulic stimulation.

Although well-oriented fractures exist in each potential interval, there are significant differences in fracture density and orientation between intervals. In the shallowest and deepest intervals (Figures 4d and 4f respectively), fractures largely dip to the SE whereas a complete pair of conjugate sets dipping NW and SE that are well oriented for normal slip are visible in the middle interval (Figure 4c). This, in conjunction with the relatively high fracture density (Figure 3), suggests that the middle interval might have the greatest fracture connectivity of the three potential stimulation intervals. In detail, fracture density and attitude strongly correlate with stratigraphic unit. In this regard, it is also worth noting that this middle interval contains the largest pre-existing fluid flow anomaly as identified in TPS logs (Figure 3).

5. CONCLUSION

Fractures that appear well oriented for normal slip exist throughout well 27-15, consistent with normal faults mapped at the surface and the orientation of S_{hmin} determined from borehole deformation revealed in the image logs. Although there are differences in the density and range of fracture orientations between the three stimulation intervals being considered, all potential stimulation intervals contain both natural fractures well oriented for normal slip and temperature anomalies indicating the presence of permeable natural fractures accessible to hydraulic

stimulation. Thus all intervals appear to have key geological characteristics necessary to induce self-propping shear failure to increase formation permeability. However, direct determination of the 3-D stress regime at Desert Peak and the magnitudes of fluid pressure at which slip would be induced during an EGS stimulation have not yet been determined pending completion of a mini-hydraulic fracturing experiment coupled to a geomechanical analysis of breakout width and rock strength.

6 ACKNOWLEDGMENTS

We would like to acknowledge collaboration and support from Ormat Technologies, Inc. that made this research possible, in particular Stuart Johnson, Gene Suemnicht, Peter Drakos, and Mark Tibbs. Joe Henfling, Dennis King and Douglas Blankenship of Sandia National Lab provided critical support during well logging operations, maintenance and modification of the ABI85; Joe Svitek of the U.S. Geological Survey played a critical role in fielding the ABI85. The Desert Peak EGS project is supported by the U.S. Department of Energy, Assistant Secretary for Energy Efficiency and Renewable Energy, under DOE Grant No. DE-FC36-02ID14406 and the USGS Energy Program.

6. REFERENCES

Barton, C.A., Zoback, M.D., and Moos, D., (1995), Fluid flow along potentially active faults in crystalline rock: *Geology*, v. 23, no. 8, p. 683-686.

Barton, C., Hickman, S., Morin, R., Zoback, M.D., and Benoit, R., (1998), Reservoir-scale fracture permeability in the Dixie Valley, Nevada, geothermal field: *in* Holt, R. M. et al. (eds.), *Rock Mechanics in Petroleum Engineering*, v. 2: Richardson, TX, Society of Petroleum Engineers, v. 2, p. 315-322.

Brown, S.R., (1987), Fluid flow through rock joints: Effects of surface roughness:, *Journal of Geophysical Research*, v. 99, 9373-9390.

Cheung, P.S., (1999), Microresistivity and ultrasonic imagers: tool operations and processing principles with reference to commonly encountered image artifacts: *in* Lovell, M.A., Williamson, G., & Harvey, P.K., (eds.),, *Borehole Imaging: Applications and Case Histories*, Geological Society, London, Special Publications, v. 159, p. 45-57.

Cornet, F.H., (1989), Survey by various logging techniques of natural fractures intersecting a borehole: *Proceedings of the 3rd International Symposium on Borehole Geophysics for Mining, Geotechnical, & Groundwater Applications*, Vol. II, p. 559-569, Mining & Geotechnical Logging Society of SPWLA.

Davatzes, N.C. and Hickman, S., (2005), Controls on fault-hosted fluid flow: Preliminary results from the Coso Geothermal Field, CA: *Geothermal Resources Council Transactions*, v. 29, p. 343-348.

Davatzes, N.C. and Hickman, S., (2009), Stress, fracture, and fluid flow analysis using acoustic and electrical image logs in hot fractured granites of the Coso Geothermal Field, CA. *in* Pöppelreiter, M. (ed.), *AAPG Special Publication: Borehole and Dip Meter Technology, Chapter 24: Structural Applications: Stress in Basement* (in press).

Davatzes, N.C. Hickman, S.H., and Sheridan, J., (2006), Section 2.1 Fracture and Stress Analysis: *in* Rose, P., Hickman, S., McCulloch, J., Davatzes, N.C., Moore, J.M., Kovac, K., Adams, M., Mella, M., Wannamaker, P., Julian, B., Foulger, G., Swenson, D., Gosavi, S., Bhat, A., Richards-Dinger, K., Monastero, F., Weidler, R., Baisch, S., Ghassemi , A., Kohl, T., and Megel, T., 2006, *Progress Report for Year Ending December 31, 2005: Creation of an Enhanced Geothermal System through Hydraulic and Thermal Stimulation*: Report to DOE, grant # DE-FC07-01ID14186, 239 p., p. 11-37.

Drury, M.J., Jessop, A.M., and Lewis, T.J., (1984), The detection of groundwater flow by precise temperature measurements in boreholes: *Geothermics*, v. 13, no. 3, p. 163-174.

Drury, M.J. and Jessop, A.M., (1987), The effect of a fluid-filled fracture on the temperature profile in a borehole: *Geothermics*, v. 5, no. 1, p. 145-152.

Evans, K.F., Genter, A., and Sausse, J., (2005), Permeability creation and damage due to massive fluid injections into granite at 3.5 km at Soultz: 1. Borehole observations: *Journal of Geophysical Research*, v. 110, p. 1-19.

Faulds, J.E., and Garside, L.J., (2003), Preliminary geologic map of the Desert Peak – Brady geothermal fields, Churchill County, Nevada: *Nevada Bureau of Mines and Geology Open-File Report 03-27*.

Hickman, S., Zoback, M.D., Benoit, R., (1998), Tectonic controls on fault-zone permeability in a geothermal reservoir at Dixie Valley, Nevada, in *Rock Mechanics in Petroleum Engineering, Vol. 1*, R. M. Holt et al. (eds.), Soc. Petroleum Eng., Richardson, TX., 79-86.

Hickman, S., Zoback, M.D., Barton, C., Benoit, R., Svitek, J. and Summers, R., (2000), Stress and

permeability heterogeneity within the Dixie Valley geothermal reservoir: Recent results from well 82-5, *Proceedings 25th Workshop on Geothermal Reservoir Engineering*, Stanford Univ., Stanford, CA, p. 256-265.

Ito, T. and Zoback, M.D., (2000), Fracture permeability and in situ stress to 7 km depth in the KTB scientific drillhole, *Geophysical Research Letters*, 27, 1045-1048.

Lutz, S., Moore, J., Jones, C., Suemnicht, G., and Robertson-Tait, A., (2009), Geological and structural relationships in the Desert Peak Geothermal System, Nevada: Implications for EGS development, *Proceedings 34th Workshop on Geothermal Reservoir Engineering*, Stanford Univ., Stanford, CA, SGP-TR-187.

MIT (2006), *The future of geothermal energy: Impact of enhanced geothermal systems (EGS) on the United States in the 21st century*, Cambridge, MA, Massachusetts Institute of Technology.

Moos, D. and Zoback, M.D., (1990), Utilization of observations of well bore failure to constrain the orientation and magnitude of crustal stresses: Application to continental, deep sea drilling project, and ocean drilling program boreholes, *Journal of Geophysical Research*, v. 95, p. 9305-9325.

Peska, P. and Zoback, M.D., (1995), Compressive and tensile failure of inclined wellbores and determination of in situ stress and rock strength. *Journal Geophysical Research*, v. 100, pp. 12791–12811.

Robertson-Tait, A., Lutz, S.J., Sheridan, J., and Morris, C.L., (2004), Selection of an interval for massive hydraulic stimulation in well DP 23-1, Desert Peak East EGS project, Nevada. *Proceedings, 29th Workshop on Geothermal Reservoir Engineering*, Stanford University, January 26-28, 2004, SGP-TR-175.

Sorey, M.L., (1971), Measurement of vertical groundwater velocity from temperature profiles in wells: *Water Resources Review*, v. 7, p. 963-970.

Teufel, L.W., (1987), Permeability changes during shear deformation of fractured rock, *in* Balkema, A.A. (ed) *28th Symposium on Rock Mechanics*: Rotterdam, Netherlands, 473-480.

Willis-Richards, J., Watanabe, K., and Takahashi, H. (1996), Progress toward a stochastic rock mechanics model of engineered geothermal systems. *Journal Geophysical Research*, v. 101, 17481-17469.

Zoback, M.D., Barton, C.A., Brudy, M., Castillo, D.A., Finkbeiner, T., Grollimund, B.R., Moos, D.B., Peska, P., Ward, C.D., and Wiprut, D.J., (2003), Determination of stress orientation and magnitude in deep wells: *International Journal of Rock Mechanics and Mining Sciences*, v. 40, p.1049-1076.